Environmental Science Nano

Accepted Manuscript

ROYAL SOCIETY OF CHEMISTRY

rsc.li/es-nano

NANO IMPACT

This study presents for the first time the use of environment-friendly Poly (amic) acid (PAA) to synthesize polymer-supported gold (AuNPs) and silver nanoparticles (AgNPs). PAA shows great potential as both reductant and stabilizer of AuNPs and AgNPs, with the resultant nanoparticles retaining their catalytic and antimicrobial activity. This environment-friendly approach utilizing the tunable properties of PAA opens a new frontier for nanomaterials that can be used for catalysis, filtration, sensors and other applications.

Graphical abstract

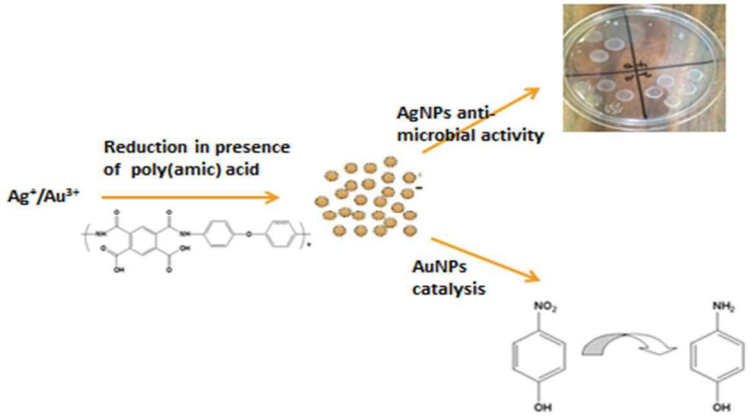

SYNTHESIS, CATALYTIC, ANTIMICROBIAL AND CYTOTOXICITY EVALUATION OF GOLD & SILVER NANOPARTICLES USING BIODEGRADABLE, π-CONJUGATED POLYAMIC ACID

Victor M. Kariuki [a], Idris Yazgan [a], Ali Akgul[c] Andrzei Kowal[d], Magdalena Parlinska[e] and Omowunmi A. Sadik [a, *]

[a]Department of Chemistry Center for Advanced Sensors & Environmental Systems (CASE) State University of New York at Binghamton P.O Box 6000 Binghamton, NY, 13902

[c] Department of Basic Sciences, College of Veterinary Medicine, Mississippi State University

[d] Institute of Non-ferrous Metals Division in Poznan, Central Laboratory of Batteries and Cells, Poznan, Poland

[e] Facility for Electron Microscopy & Sample Preparation, University of Rzeszow, Rzeszow, Poland

[*b] *Corresponding author:osadik@binghamton.edu*

ABSTRACT

We hereby report a rapid, simple, and one pot synthesis of silver nanoparticles (AgNPs) and gold nanoparticles (AuNPs) using conductive, electroactive and biodegradable. Poly (amic)acid (PAA) polymer as both the reductant and stabilizer. The synthesized AgNPs and AuNPs were characterized using transmission electron microscopy (TEM), High resolution HRTEM, energy dispersive spectroscopy (EDS), X-ray diffraction (XRD) and ultra-violet visible spectroscopy (UV-Vis). UV-VIS spectra exhibit major peaks at 440nm and 535nm for AgNPs and AuNPs respectively. The XRD patterns revealed four diffraction peaks at 38.12˚, 44.07˚, 64.27˚, and 77.22° that can be indexed to the (111), (200), (220), and (311) planes of face-centered cubic (fcc) silver crystallites respectively. The size of the crystallites along the [111] direction was estimated to be 4.2±0.5nm, which is in agreement with the TEM result. The effect of temperature on the formation of AgNPs in the presence of PAA was investigated and found to be significant at 100℃, resulting in silver-polyamic acid nanocomposite without altering the fcc crystal pattern. The prepared AuNPs and AgNPs were found to exhibit catalytic activity towards 4-nitrophenol and methylene blue with a rate constant of 5.2 $\times 10^{-3}$ S^{-1} and 1.09×10^{-2} S^{-1} respectively. Finally, the synthesized AgNPs exhibit excellent antibacterial activity against Gram negative (*E coli* DH5 Alpha, *E.coli* 25922, *Aeromonas hydrophilia* & *Pseudomonas aeruginosa*) and gram positive (*Listeria monocytogenes* strains F2365 and HCC7 and *S. epidermidis*) bacteria in addition to modest cytotoxicity against non-cancerous immortalized IEC-6 and cancerous Caco-2 cell lines.

1.0 INTRODUCTION

Gold and silver nanoparticles have attracted considerable surge in research interest due to their various inherent advantages such as the ease of synthesis, high chemical stability and size-dependent optical, electronic, and catalytic properties. This has led to diverse applications including chemical/biological sensing, surface-enhanced Raman scattering, (nano) electronics, catalysis, drug delivery, sensors, and antibacterial serum[1-7]. However due to their specific surface energy, they tend to agglomerate easily resulting in the loss of nano-particular characteristics. One strategy to prevent aggregation of the nanoparticles is to utilize appropriate stabilizers. An excellent stabilizer must not mask the properties of the nanoparticles. It has been shown that the presence of a densely packed capping layer on metal nanoparticle surface may compromise the

catalytic activity as surface active sites become inaccessible and compact layer introduces steric hindrance for the inward diffusion of reactants to nanoparticle surface and outward diffusion of reaction products [8-10]

Moreover, there has been a recent surge in interest in the synthesis and applications of Intrinsically conducting polymers (ICPs) with incorporated metal nanoparticles[11, 12]. Several Intrinsically conducting polymers such as polyaniline[13, 14], polypyrrole[15] have been used as reductants and stabilizers of gold and silver nanoparticles. However, application of polyaniline [16] is limited due to its low processability, insolubility in a wide range of solvents and its non-biodegradability. Notably metal nanoparticles supported by PANI alone are not stable; forming aggregates in solution even after standing for a few minutes[17]. Similarly, polypyrrole is insoluble in a wide range of solvents.

Intrinsically conducting polymer molecules containing active groups and a considerable level of steric hindrance are believed to be more advantageous as stabilizers of metal nanoparticles. PAA, an electroactive[18, 19], conductive[18, 20] and biodegradable[21, 22] polymer contains numerous amounts of amide and carboxyl functional groups. Also, PAA has a high cation-complexing abilities[19, 23, 24], implying that polymeric metal complexes can easily be generated by in-situ reactions between PAA and labile salts of noble metals. Unlike other ICPs such as polyaniline and polypyrrole, PAA has excellent biodegradable characteristics hence will not introduce any environmental toxicity. In this work, we used π-conjugated, biodegradable PAA as support and reducing agent to prepare AuNPs and AgNPs. The resulting nanoparticles exhibit excellent dispersibility and stability. Most importantly, the resulting AuNPs demonstrate apparent catalytic activity for the reduction of 4-nitrophenol to 4-aminophenol while the AgNPs demonstrate excellent antimicrobial and catalytic activity.

2.0 MATERIALS AND METHODS

2.1 Reagents

Silver nitrate ($AgNO_3$), gold(III)iodide(AuI_3), pyromellitic dianhydride (PMDA), 4'4 oxydianiline, dimethyformamide (DMF), 4-nitrophenol, methylene blue, dimethyl acetamide (DMAC), Muller Hinton Broth, Alamar Blue and sodium borohydride ($NaBH_4$) were purchased

from Sigma Aldrich St. Louis MO, USA. All reagents were analytical grade and used without further purification.

2.2 Synthesis of Poly (amic) acid-PAA

210.25mg of 4'4-oxydianline was added into a vial followed by 3.5 to 4 mL of DMF dispensed using a syringe. This mixture was stirred until complete dissolution of ODA was observed. This was followed by the addition of 229.02 mg PMDA and 1 mL of DMAC. The vial was then covered with either a box container or aluminum foil after capping and stirred for 12 hours. The resulting PAA was a yellow viscous solution.

2.3 Preparation of Gold nanoparticles (AuNPs)

2.88mg of AuI_3 was dissolved in 5 ml DMF and PAA solution was added. The reaction mixture was observed at room temperature with a solution of AuI_3 in DMF used as control. The setup was monitored over time and UV-VIS spectroscopy used to characterize the formation of AuNPs.

2.4 Preparation of Silver nanoparticles (AgNPs)

The following set ups were used for the synthesis of silver nanoparticles:

A-5mg of $AgNO_3$ + 5ml DMF +PAA (0.21M) was monitored at room temperature for 5 days.

B-5mg of $AgNO_3$ + 5 ml DMF+ PAA (0.21M) was monitored at 70 °C for 150 minutes

C-5mg of $AgNO_3$ + 5ml DMF+ PAA (0.21M) was monitored at 100 °C for 200 minutes

2.5 Characterization

UV-VIS spectra of the synthesized nanoparticles were measured at different aging times using Hewlett Packard 8453 UV-VIS spectrophotometer from 200nm to 700nm. TEM measurements were conducted using a JEOL 2100F operating at an acceleration voltage of 200 kV. The TEM samples were prepared by dropping few drops of final products on a SiO_2 coated copper grid (TedPella) and drying under a dryer for 5 minutes. The XRD patterns were obtained using a Bruker D8 Discover XRD system operating at 40 kV and 40 mA. The diffraction patterns were recorded in θ–2θ symmetry scanning mode within the range of 30˚ to 90˚. Test samples were

prepared by dropping about 10mL silver or gold colloids on quartz plates and allowing them to dry.

2.6 Reduction of 4-nitrophenol catalyzed by PAA-synthesized AuNPs

A typical mixture for the reduction consists of a 300µL PAA-Au solution (5×10^{-5}M in water), 850µL of 4-nitrophenol (0.2mM aqueous solution) and 500 µL of freshly prepared $NaBH_4$ (25mM aqueous solution) in a 5mL glass vial. The mixture was quickly transferred to a cuvette for UV-Vis absorption measurements. Nanopure water was used as the reference. All experiments proceeded under ambient conditions.

2.7 Reduction of methylene blue catalyzed by PAA-synthesized AgNPs

The catalytic properties of PAA synthesized AgNPs was evaluated using a standard methylene blue reduction reaction. Two reaction setups were employed and monitoring was achieved using UV-Visible spectrophotometer in the range of 400nm-800nm. In first set up, 1ml of Methylene Blue (1×10^{-4}M) was mixed with excess of 32mM $NaBH_4$ and the mixture was monitored for 30 minutes. In the second setup, 1ml of Methylene Blue was mixed with excess of 32mM $NaBH_4$ in the presence of 400µl PAA synthesized AgNPs (5×10^{-5} M) and reaction was monitored for 3 minutes.

2.8 Evaluation of antimicrobial, antifungal and cytotoxic characteristic of PAA-stabilized AgNPs

Antibacterial and antifungal activity of PAA-synthesized silver nanoparticles were tested to examine how they alter the growth dynamics of gram positive and gram negative bacteria. The gram negative bacteria examined include *Escherichia coli* ATCC® 25922™, *E.coli* DH5alpha, *Aeromonas hydrophilia*, and *Pseudomonas aeruginosa*. The gram positive bacteria tested were *Staphylococcus epidermidis* ATCC® 12228™ with *Listeria monocytogenes* strains F2365 and HCC7 respectively. Antifungal activity was tested using the addition of *Trichaotum biforme* into a freshly prepared 10 µg/mL silver-nanoparticle containing Mueller Hinton Broth. While *E.coli* 25922 and *S.epidermidis* were grown in Mueller Hinton Agar, virulent type strain *L. monocytogenes* were grown in a rich medium such as brain heart infusion while Lysogeny broth

(**LB**), a nutritionally rich medium agar was used for the maintenance of the tested *E. coli DH5alpha, Aeromonas hydrophilia and Pseudomonas aeruginosa*.

The effect of PAA-synthesized silver nanoparticles on microbial growth was tested using two approaches: (i) bacteria were incubated in liquid phase (broth) and (ii) solid phase respectively. The concentrations of AgNPs used for antimicrobial activity varied for the type of bacteria within the range of 1-20 µg/mL. Turbidity test was performed by dissolving the resulting colonies in 50:50 phosphate buffer saline (PBS) buffer: Muller Hinton Broth. The absorbance of the Mueller Hinton Broth mixture was used to calculate the bacterial concentration using standard curve.

Cytotoxicity of silver nanoparticles was tested on *passage 31-35* IEC-6 [DMEM medium with 0.1µg/mL Bovine insulin, 10% FBS and 1% penicillin & streptomycin mixture] and *passage 85-90* Caco-2 cell lines [DMEM medium with 10% FBS and 1% penicillin & streptomycin mixture]. While 10 µg/mL AgNPs was used for Caco-2 cells, the nanoparticles were used at 5, 10, 15 and 30µg/mL for IEC-6 cells. Toxicity was evaluated with presto blue® dye and comparison of final confluence of control and silver nanoparticle treated wells were carried out. The details are described in the supplementary information **S10.**

3.0 RESULTS AND DISCUSSION

3.1 Reaction Mechanism for the Formation of Nanoparticles

Polymers such as polypyrrole and polyaniline are readily transformed to their respective oxidized forms using in-situ reduction of metal ions such as Pd^{2+} and Au^{3+} [25, 26]. In this study, we used PAAs which possess electron donating properties[23] to reduce Au^{3+} to Au^{0} and Ag^{+} to Ag^{0}. The oxidized polymer also protects and stabilizes the AuNPs and AgNPs in accordance with the following reactions:

$$Au^{3+} + 3PAA^{0}_{(s)} \longrightarrow Au^{0} + 3PAA^{+} \quad (1)$$

$$Ag^{+} + PAA^{0}_{(s)} \longrightarrow Ag^{0} + PAA^{+} \quad (2)$$

The use of PAA results in the effective reduction of gold and silver salts while also stabilizing the nanoparticles, thus providing excellent robustness against agglomeration (Figure 1)[27]. PAAs

possess lone pairs of electrons on the nitrogen species capable of adsorbing onto the nanoparticles surface and stabilizing them via steric hindrance (Figure 1)[28].

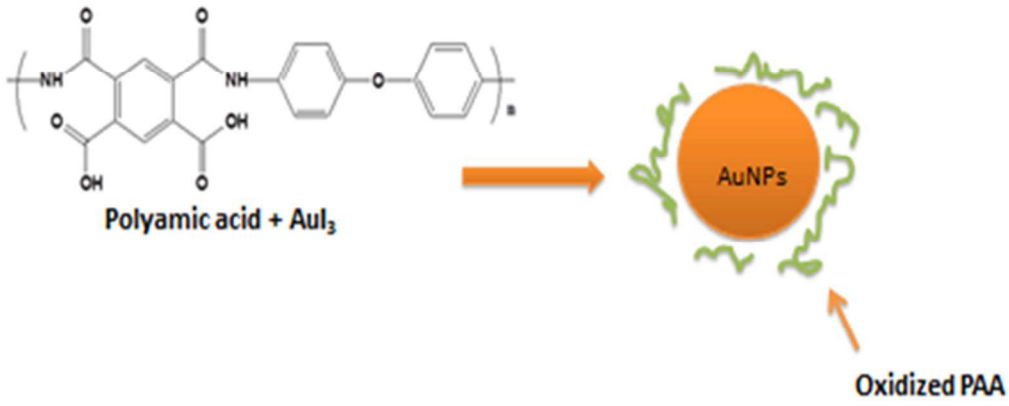

Figure 1: Stabilization mechanism of AuNPs by PAA

3.2 Optical Characterization

It is well known that nanoparticles exhibit distinct color in aqueous solution due to excitation of surface plasmon vibrations (SPR)[29]

Figure S1A shows the pictograph for the mixture of gold and PAA with color changing from yellow to purple. A similar setup without the PAA remained yellow throughout the experiment. These results indicate the formation of AuNPs. Similarly, the formation of AgNPs was accompanied by color changes over time; with color changing from pale yellow of the PAA matrix to bright yellow, to light reddish brown and finally to deep reddish brown **(Figure S1B, C & S2)**. This was observed in all the setups at different temperatures (room temperature, 70 ˚C and 100 ˚C).

The solutions presented a favorable homogeneity without precipitation indicating that the nanoparticles were stable and well-dispersed in the PAA medium. The origin of the color changes is derived from the different states of the SPR of the nanoparticles at their characteristic wavelengths which was registered by the UV-Vis absorption spectra[30].

3.3 UV-Vis Characterization

As evident in **Figure 2A**, AuNPs absorption band appeared at 535nm. It can be concluded that the band is due to the SPR of the gold nanoparticles at 510-525nm in aqueous system[31]. It is evident that the absorption band of PAA protected gold nanoparticles was shifted compared with the calculated value. Gold nanoparticles of 5–50 nm show a sharp absorption band in the 520–530 nm region[32]. The size deduced from UV-VIS data agrees with TEM and XRD characterization. In the case of AgNPs, reduction occurred slowly at room temperature and up to 5 days was needed to observe any noticeable color change **(Fig S1C)**. At 70˚C, it took 15 minutes **(Fig S2)** to record any color change while only 5 minutes was needed to observe any visible color change at 100 °C **(Fig S1B)**. This trend implies that higher temperature speeds the formation of nanoparticles.

The colloids formed were stable over two months with no precipitation. The characteristic brown color of silver solutions provided a noticeable spectroscopic signature to indicate their formation[33]. The color of the silver colloid is attributed to the collective oscillation of free conduction electrons induced by an interacting electromagnetic field[34]. SPR bands were centered at 440 nm. The bands were broad and intensity increased with time indicating increase in production of nanoparticles with temperature. At 70 °C (**Fig S3**), the plasmon intensity of the reaction at 65 minutes was near to that at 90 minutes. Similarly at 100 °C (**Fig 2B**), the SPR at 45 minutes was near that at 55 minutes. This signifies the completion of the reaction. It is possible to determine the efficiency as a function of time using normalized UV/VIS spectra. **Figure 2C** shows the time-dependent conversion of Ag^+ to AgNPs at 100˚C. After 35 minutes, the reaction levelled off at 89% efficiency.

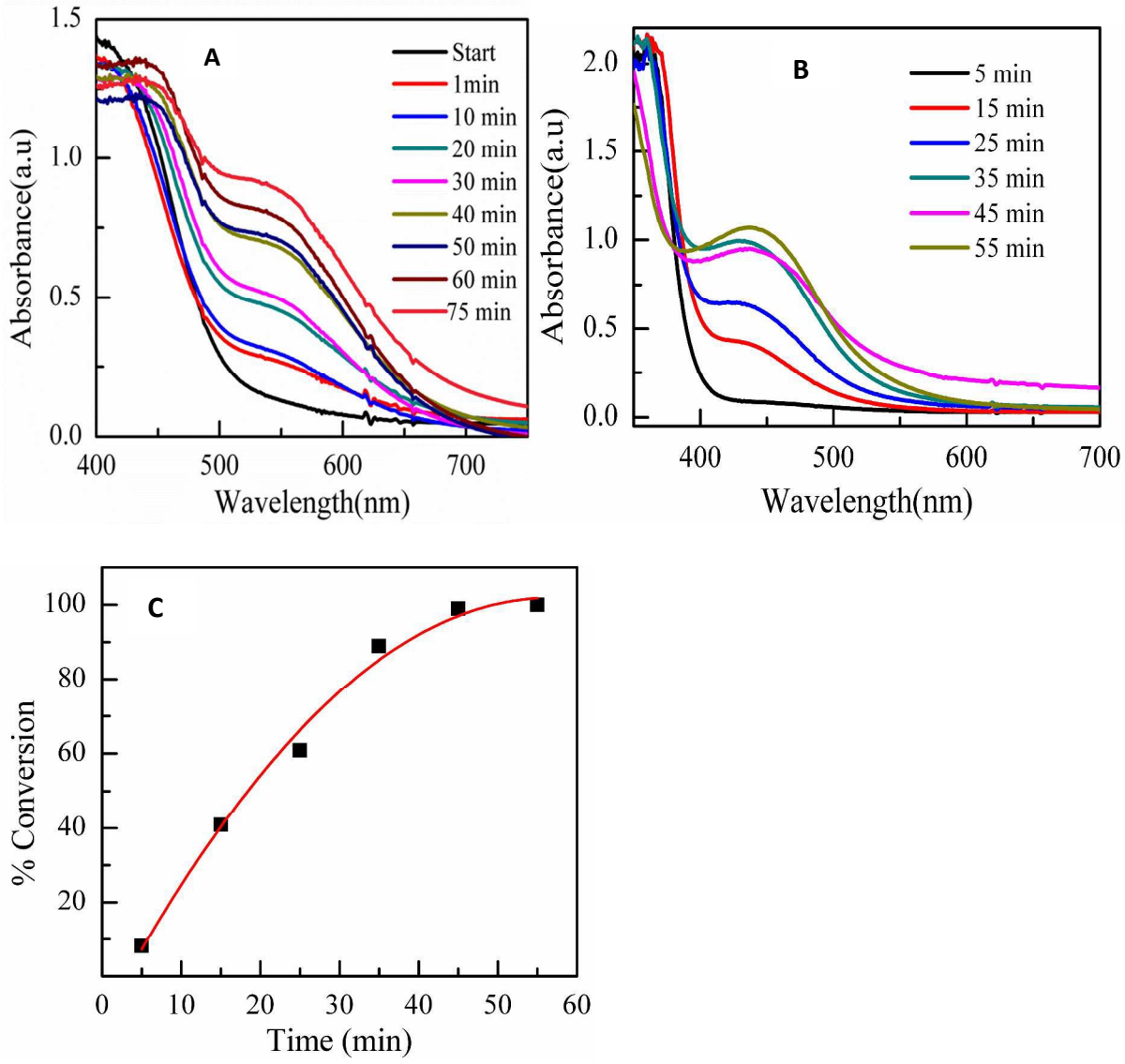

Figure 2: Time evolution of UV-vis absorption spectra of reaction mixture **A**-AuNPs at room temperature, **B**- AgNPs at 100˚C **C**-Progress of reaction for AgNPs formation at 100˚C

3.4 Morphological Investigation

3.4.1 Gold Nanoparticles

Figure 3A is the TEM micrographs of AuNPs synthesized using PAA. This revealed that the particles are much dispersed with elliptical shapes (dark contrast objects) confirming that PAA act as both stabilizer and reducing agent. Statistical analysis based on over one hundred nanoparticles shows that the majority of the gold nanoparticles were approximately 10nm in

diameter. This is manifested by core size histogram shown in **Figure 3B**. Furthermore, from the high-resolution TEM image shown in **Figure 3C**, one can see the clearly defined lattice fringes with a spacing of 0.24 nm, which are consistent with the (111) crystallographic planes of face-centered cubic (fcc) gold, indicating the highly crystalline nature of the gold nanoparticles synthesized. The EDS spectra confirmed that AuNPs were formed. The Cu in the EDX spectrum is from the TEM grids.

Figure 3E shows the XRD studies of the PAA stabilized nanoparticles which displayed four diffraction peaks at 38.12˚, 43.07˚, 64.47˚, and 77.22˚ that can be indexed to the (111), (200), (220), and (311) planes of fcc gold crystallites, respectively. The size of the crystallites along the [111] direction was estimated to be 9.7±0.5 nm based on the calculation using the Scherrer equation. The XRD data are in good agreement with the TEM result in **Figure 3A**.

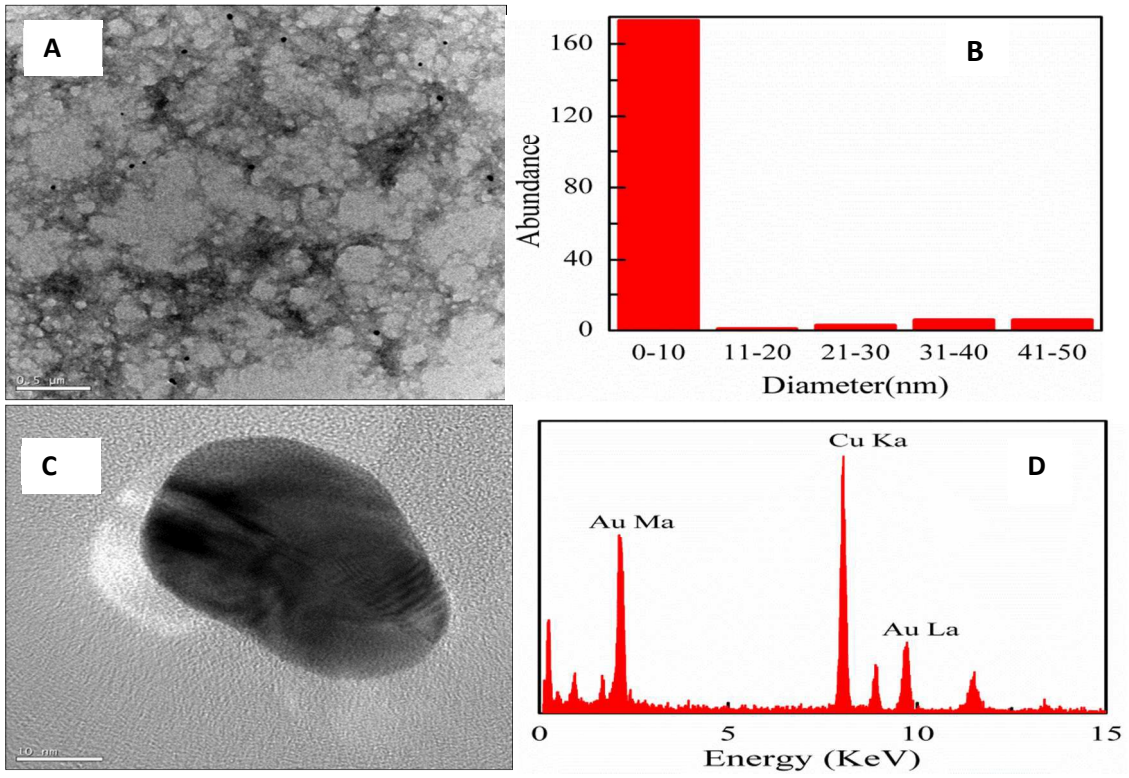

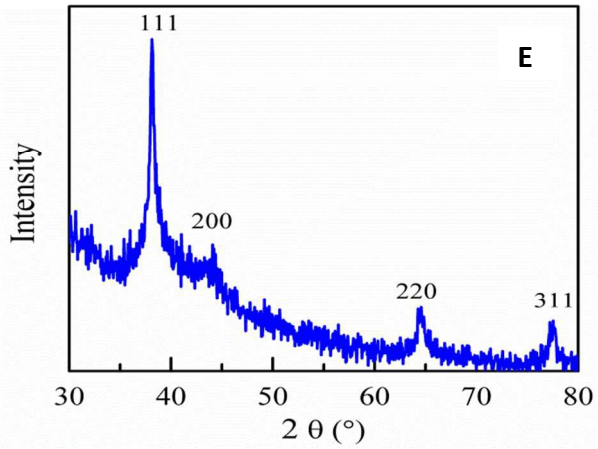

Figure 3:TEM micrographs(A),High resolution TEM micrograph(C) ,Particle size histogram(B) EDX spectrum(D) and XRD patterns(E) of PAA-Stabilized AuNP.

3.4.2 Silver Nanoparticles

TEM micrographs of silver nanoparticles at room temperature showed very well dispersed AgNPS (**Figure 4A**) synthesized using PAA as stabilizer and reductant. The analysis of particle size distribution revealed that majority of the particles are ~3.8nm in diameter (**Figure 4B**). HRTEM images showed 5 fold symmetry twinned nanoparticles. The XRD patterns revealed four diffraction peaks at 38.12 °, 44.07 °, 64.27 ° and 77.22 ° that can be indexed to the (111), (200), (220), and (311) planes of fcc silver crystallites, respectively. The size of the crystallites along the [111] direction was estimated to be 4.2 ± 0.5 nm based on the calculation using the Scherer equation; also in good agreement with the TEM result in **Figure 4A**.

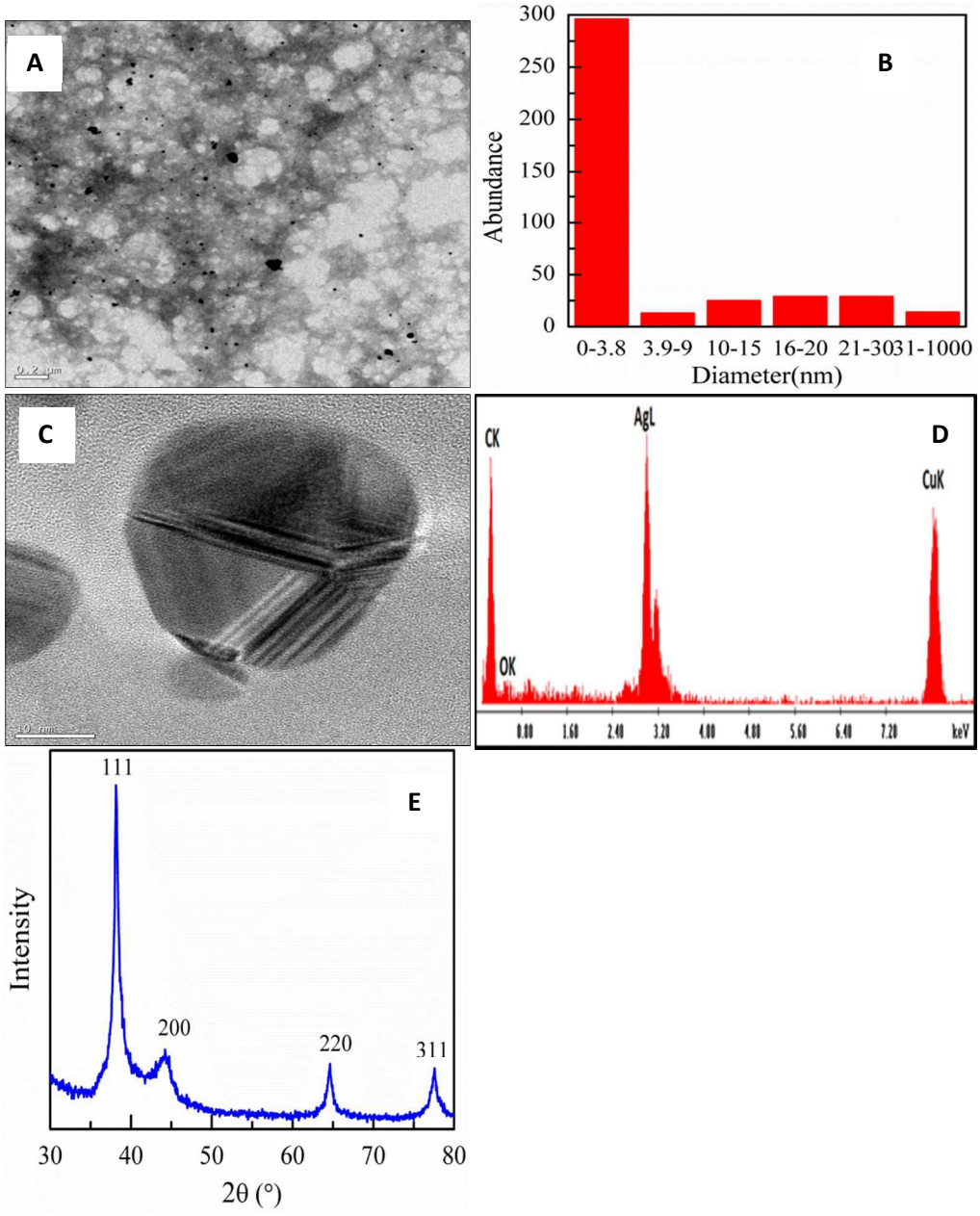

Figure 4: TEM micrographs (A), size distribution histogram (B) High Resolution TEM micrograph(C), EDS Spectra (D) and XRD pattern (E) of PAA stabilized AgNPs at room temperature

At 70˚C there was no significant change in the size distribution **(Figure S4)** as AgNPs of 4nm size were formed. Particles were also highly crystalline as seen in the XRD having FCC patterns with diffraction peaks **(Figure S4)** that were indexed to (111), (200), (220) and (311).

At 100˚ C, PAA-AgNPs composites were formed with dispersed AgNPs trapped within the polymer matrix as shown in **Figures 5** A and B. High resolution TEM micrograph (**Figure 5C**) revealed highly crystalline overlapping particles with an fcc pattern as confirmed by XRD pattern (**Figure 5E**).

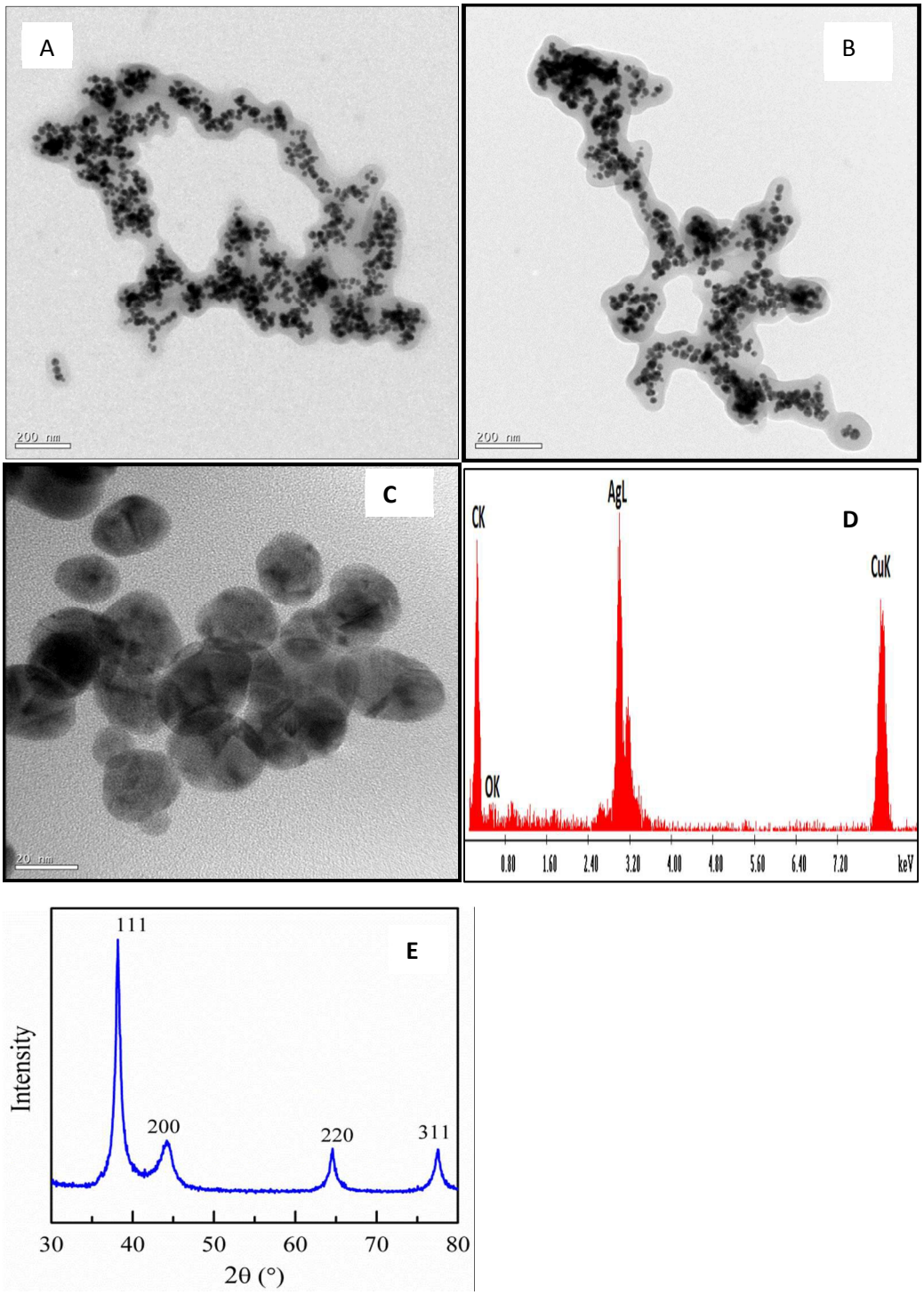

Figure 5: TEM micrograph (A and B), High Resolution TEM micrograph(C), EDS spectra (D) XRD patterns (E) of PAA stabilized AgNPs at 100˚C

3.5 Catalytic activity of PAA stabilized AuNPs

As stated earlier, an effective way to prevent aggregation is to utilize appropriate stabilizers. However, it has been shown that the presence of densely packed capping layer on the metal nanoparticle surface may compromise the catalytic activity since surface active sites become inaccessible[8, 10, 17, 35]. Therefore, it was necessary to confirm whether the AuNPs stabilized with PAA retained their catalytic activity. The reduction of 4-nitrophenol into 4-aminophenol in the presence of excessive $NaBH_4$ was chosen as a model to test the catalytic activity of the PAA stabilized AuNPs. This reaction has been used extensively as a benchmark to quantify the catalytic activity of various metallic nanoparticles since the reaction dynamics can be easily monitored using UV-Vis absorption spectroscopy[17, 36]. Upon the addition of excessive $NaBH_4$ into a 4-nitrophenol solution, the color of the solution changed quickly from light yellow to green yellow.

Figure 6a depicts the UV-Vis absorption spectra of 4-nitrophenol solution in the presence of PAA stabilized. AuNPs collected at different reaction intervals. At the beginning of the reaction, the solution exhibited a major absorption peak at 400nm and another band at 300nm. This is due to formation of 4-nitrophenolate anions under basic conditions. The intensity of the peak at 400nm decreased quickly with time and at same time, the intensity of the peak at 300nm increased. The rate of reduction is monitored by the disappearance of this peak. The UV-Vis spectra shows an isosbestic point (around 320nm) suggesting that the catalytic reduction of 4-nitrophenol gives 4-aminophenol only, without byproduct. The reaction appeared to complete within 500s. The accompanying color change is shown in **Figure S5**. The absorption peak at 300nm is characteristic of 4-aminophenol[36, 37]. The graph clearly indicates the effective reduction of 4-nitrophenol into 4-aminophenol in the presence of PAA synthesized AuNPs.

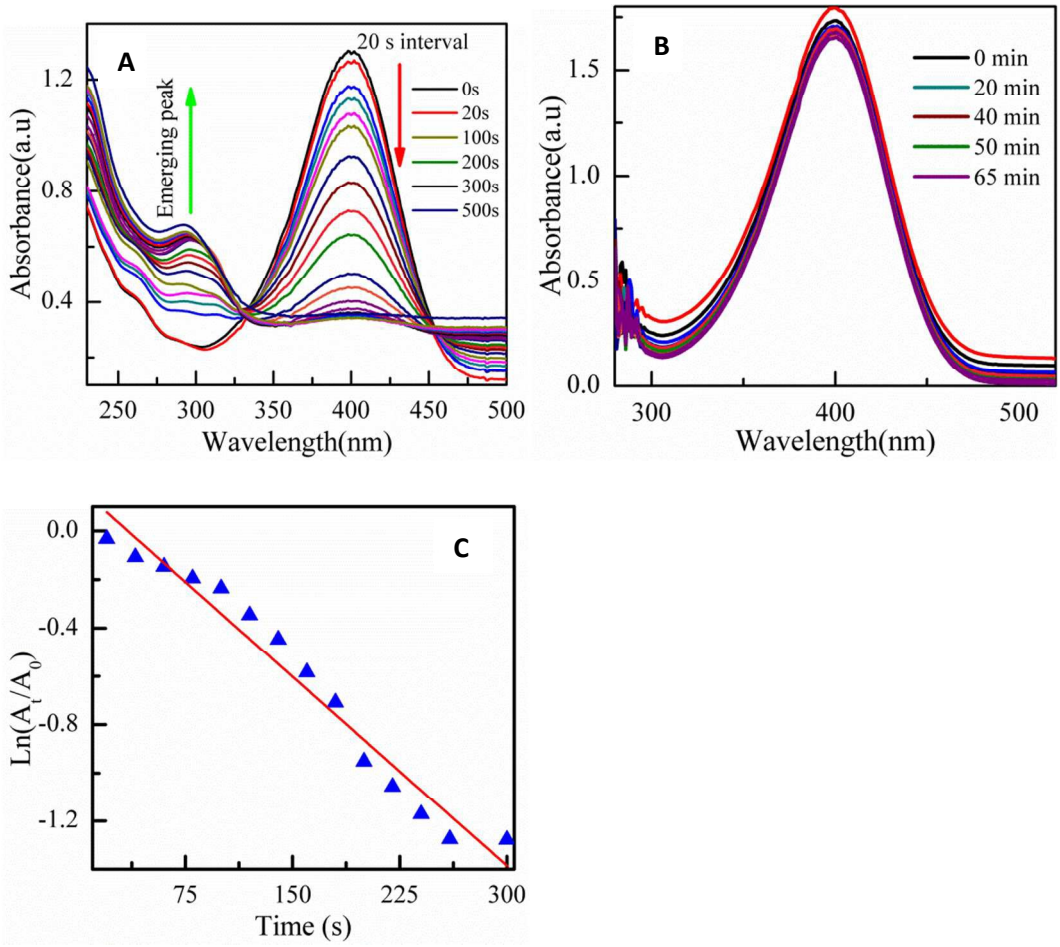

Figure 6: (A) Time dependent UV-vis absorption spectra of the reduction of 4-nitrophenol by $NaBH_4$ in the presence of PAA-stabilized AuNPs. (B) Time dependent UV-vis absorption spectra of the reduction of 4-nitrophenol by $NaBH_4$ in the absence of PAA-stabilized AuNPs (C) Plot of ln (A_t/A_0) as a function of time for the reaction catalyzed by PAA-stabilized AuNps.

Since this reaction was conducted under a large excess of $NaBH_4$, the reaction rate was nearly independent of the $NaBH_4$ concentration and consequently the kinetics can be modeled by a quasi-first order process with respect to the concentration of 4-nitrophenol. Therefore the rate constant for the reduction process was determined by measuring the change in absorbance at 400nm as a function of time. **Figure 6C** depicts the plot of ln (A_t/A_0) as a function of reaction time (t), where A_t and A_0 are absorption intensities at time t and 0 respectively. The kinetic rate constant (k) of 5.2 $X10^{-3}$ S^{-1} was derived from the linear regression of the experimental data.

An additional control experiment was setup by adding only $NaBH_4$ to 4-nitrophenol but without PAA stabilized gold nanoparticles. The UV-Vis absorption profiles remained unchanged for up to 60 minutes, indicating that no reduction of 4-nitrophenol into 4-aminophenol occurred in the absence of PAA stabilized gold nanoparticles **(Figure 6B).**

3.6 Catalytic activity of PAA-synthesized AgNPs

The reduction of methylene blue (MB) has been used extensively as a benchmark to quantify the catalytic activity of various metallic nanoparticles since the reaction dynamics can be easily monitored using UV-Vis absorption[38, 39]. Addition of PAA synthesized AgNPs and excess of 32mM $NaBH_4$ into MB solution at room temperature produced a color change from blue to colorless. MB exhibits a peak maxima at 658nm which corresponds to n-π* transition and a shoulder at 614nm[40, 41]. In presence of $NaBH_4$, the reaction barely takes place as shown by the constant intensity of the absorption band at 664nm **(Figure S7A)**. However in presence of AgNPs, MB undergoes a faster reduction to form leucomethylene blue **(Figure S6 and S7B)**, and methylene blue absorption peak at 664nm decreases rapidly within 3 minutes. This confirms the catalytic activity of the PAA-synthesized AgNPs. The first order kinetics modeling reveals a rate constant of 1.09×10^{-2} S^{-1}.

3.7 Antimicrobial Activity and Cytotoxicity of PAA-stabilized Silver Nanoparticles

As detailed in **Figure 7**, AgNPs showed antibacterial activity on *Escherichia coli* DH5 Alpha (gram negative), and *Listeria monocytogenes* strains F2365 and HCC7 (gram positive) as well as on *E.coli* 25922 and *S.epidermidis* (results are shown in **Supplementary Figure S9**) and *Aeromonas hydrophilia* (gram negative) and *Pseudomonas aeruginosa* (gram negative) (results are shown in **Supplementary Figure S11**). Unlike the response of *E.coli* 25922 (gram negative) and *S.epidermidis* (gram positive) to silver nanoparticles, *Escherichia coli* DH5 Alpha, and *Listeria monocytogenes* (strains F2365 and HCC7) showed different responses to AgNPs toxicity. The treatment decreased the *E.coli* DH5 colonies count by 75% in comparison to the control while the treatment *Listeria monocytogenes* (F2365 and HCC7) colonies with AgNPs decreased their sizes by over 35%.

However, in all cases AgNPs exhibited antibacterial activity against these gram (+) and gram (-) bacteria. The difference of how AgNPs showed their anti-bacterial activities can be explained in three ways, (i) type of bacteria, (ii) medium differences and/or (iii) age and concentration of microbial inoculums. However, it should be mentioned that the age of silver nanoparticles also made a difference in addition to these three reasons. One week old silver nanoparticles were tested for *E.coli* 25922 and *S. epidermidis*, and it was observed that the antibacterial activity decreased by about 10 percent within 3 months (data not shown); the results presented here are from 3-months old nanoparticles. Different concentrations of silver nanoparticles did not show dramatic changes because autoclaving AgNPs caused agglomeration, which was not seen before autoclave. The AgNPs did not show even distribution after 1µg/mL concentration, which was shown in **Supplementary S12**.

In summary, the results clearly showed that the synthesized silver nanoparticles exhibit strong antibacterial activity through either decreasing the colony number or reducing the size of formed-colonies for bacteria [detailed in **Figure S9**] and slight inhibitory effects on fungi **(Figure S8**).

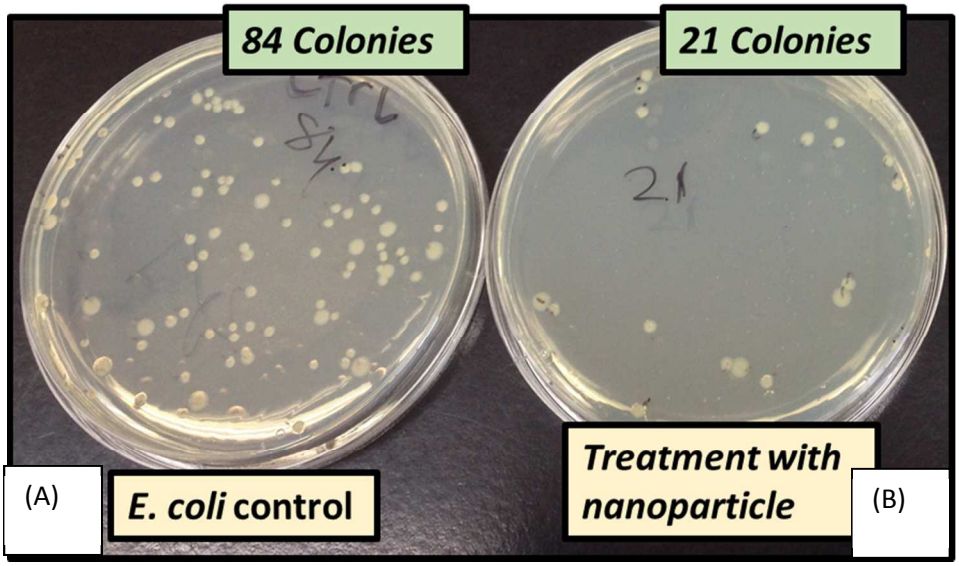

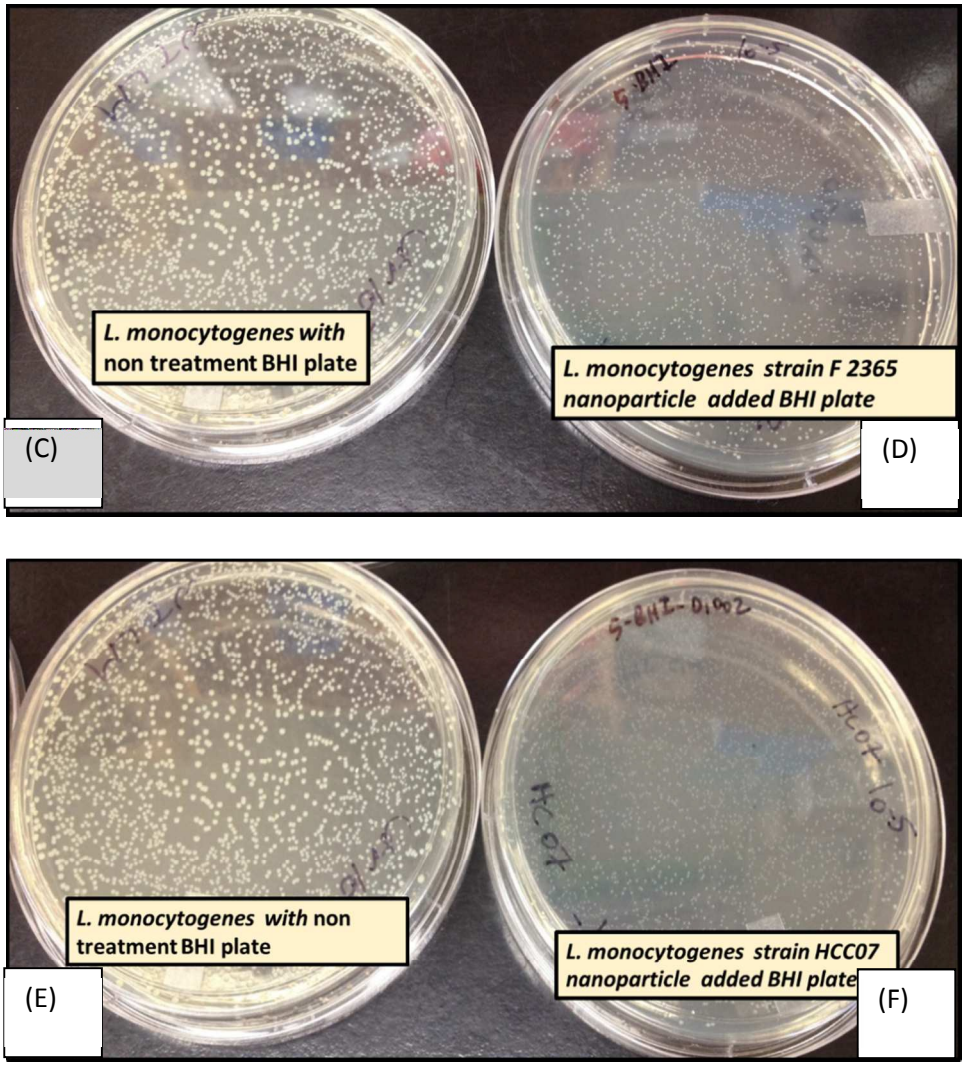

Figure 7: Growth of *E. coli* upon treatment with 10 µg/ml of silver-nanoparticle agar [B], and control non-treated LB plate [A]. Antibacterial activity recorded for *L. monocytogenes* strain F2365 upon treatment with 10 µg/ml of nanoparticle agar: [d] and [c] control LB plate, and *L. monocytogenes* strain HCC07 [f] and control non-treated plate [e]. For more details on this set up, refer to **S11.**

All cytotoxicity results are displayed in supporting information **(S10)**. Fig S10 **A** and **B** depict a change in growth pattern of Caco-2 cells in response to AgNPs treatment while IEC-6 cells showed a 5% decrease in confluence. **Fig S10E** shows a fluorescence based viability study: AgNPs concentration above 5µg/ml resulted in over 25% decrease in viability. This shows that the AgNPs exhibited mild cytotoxicity against non-cancerous IEC-6 cells.

4.0 CONCLUSION

We have herein reported a one-step method for the synthesis of well-dispersed AuNPs and AgNPs using PAA as both the reductant and stabilizer. The as-prepared nanoparticles were stable for over 3 months at room temperature. The nanoparticles formed had a narrow size distribution (~10nm for AuNPs and~ 5nm for AgNPs). Further temperature dependence on the formation of AgNPs revealed that PAA-AgNPs nano composites can be synthesized at 100˚C without altering the fcc crystal pattern. The utilization of biodegradable polymer eliminates the use of toxic volatile organics during the synthetic process. We have also shown that the as-prepared PAA stabilized AuNPs and AgNPs retained their catalytic activity towards 4-nitrophenol and methylene blue with a rate constant of 5.2×10^{-3} S^{-1} and 1.09×10^{-2} S^{-1} respectively. Finally, this work has also demonstrated that the AgNPs exhibited robust antimicrobial activity against *Escherichia coli*, *Staphylococcus epidermidis, Aeromonas hydrophilia, Pseudomonas aeruginosa, Listeria monocytogenes, S.epidermidis* and modest cytotoxicity against non-cancerous immortalized IEC-6 and cancerous Caco-2 cell lines.

ACKNOWLEDGEMENTS

The authors acknowledge the National Science Foundation CBET 1230189 for funding. Idris Yazgan and Ali Akgul also acknowledge the support of the Turkish Government fellowship. The Regional NMR facility (600 MHz instrument) at SUNY-Binghamton is supported by NSF (CHE-0922815).

ASSOCIATED CONTENT

Supporting information

Figures S1-S11 provides additional information on synthesis, characterization, catalytic, antimicrobial and cytotoxicity of the PAA-synthesized AgNPs and AuNPs.

REFERENCES

1. S. Andreescu, J. Njagi, C. Ispas and M. T. Ravalli, *Journal of Environmental Monitoring*, 2009, **11**, 27-40.
2. I. Pastoriza-Santos and L. M. Liz-Marzán, *Nano letters*, 2002, **2**, 903-905.
3. T. K. Sau and C. J. Murphy, *Journal of the American Chemical Society*, 2004, **126**, 8648-8649.

4. R. A. Sperling, P. R. Gil, F. Zhang, M. Zanella and W. J. Parak, *Chemical Society Reviews*, 2008, **37**, 1896-1908.
5. S. Guo and E. Wang, *Analytica chimica acta*, 2007, **598**, 181-192.
6. D. Pissuwan, T. Niidome and M. B. Cortie, *Journal of controlled release*, 2011, **149**, 65-71.
7. L. Dykman and N. Khlebtsov, *Chemical Society Reviews*, 2012, **41**, 2256-2282.
8. R. M. Crooks, M. Zhao, L. Sun, V. Chechik and L. K. Yeung, *Accounts of chemical research*, 2001, **34**, 181-190.
9. R. Su, R. Tiruvalam, Q. He, N. Dimitratos, L. Kesavan, C. Hammond, J. A. Lopez-Sanchez, R. Bechstein, C. J. Kiely and G. J. Hutchings, *ACS nano*, 2012, **6**, 6284-6292.
10. M. M. Nigra, J.-M. Ha and A. Katz, *Catalysis Science & Technology*, 2013, **3**, 2976-2983.
11. S. M. Marinakos, D. A. Shultz and D. L. Feldheim, *Advanced Materials*, 1999, **11**, 34-37.
12. D. W. Hatchett, M. Josowicz, J. Janata and D. R. Baer, *Chemistry of Materials*, 1999, **11**, 2989-2994.
13. K. Mallick, M. J. Witcomb and M. S. Scurrell, *Journal of materials science*, 2006, **41**, 6189-6192.
14. H. Gu, S. Tadakamalla, Y. Huang, H. A. Colorado, Z. Luo, N. Haldolaarachchige, D. P. Young, S. Wei and Z. Guo, *ACS applied materials & interfaces*, 2012, **4**, 5613-5624.
15. X. Feng, H. Huang, Q. Ye, J.-J. Zhu and W. Hou, *The Journal of Physical Chemistry C*, 2007, **111**, 8463-8468.
16. S. Panigrahi, S. Basu, S. Praharaj, S. Pande, S. Jana, A. Pal, S. K. Ghosh and T. Pal, *The Journal of Physical Chemistry C*, 2007, **111**, 4596-4605.
17. X. Liu, L. Li, M. Ye, Y. Xue and S. Chen, *Nanoscale*, 2014, **6**, 5223-5229.
18. N. Du, C. Wong, M. Feurstein, O. A. Sadik, C. Umbach and B. Sammakia, *Langmuir*, 2010, **26**, 14194-14202.
19. D. Andreescu, A. K. Wanekaya, O. A. Sadik and J. Wang, *Langmuir*, 2005, **21**, 6891-6899.
20. N. M. Noah, M. Omole, S. Stern, S. Zhang, O. A. Sadik, E. H. Hess, J. Martinovic, P. G. Baker and E. I. Iwuoha, *Analytical biochemistry*, 2012, **428**, 54-63.
21. I. Yazgan, N. Du, R. Congdon, V. Okello and O. A. Sadik, *Journal of Membrane Science*, 2014.
22. O. SADIK, I. YAZGAN and V. KARIUKI, *Chemical Processes for a Sustainable Future*, 2014, 259.
23. M. A. Omole, V. A. Okello, V. Lee, L. Zhou, O. A. Sadik, C. Umbach and B. Sammakia, *ACS Catalysis*, 2011, **1**, 139-146.
24. V. A. Okello, N. Du, B. Deng and O. A. Sadik, *Journal of Environmental Monitoring*, 2011, **13**, 1236-1245.
25. K. Neoh, K. Tan, P. Goh, S. Huang, E. Kang and K. Tan, *Polymer*, 1999, **40**, 887-893.
26. S. Huang, K. Neoh, E. Kang, H. Han and K. Tan, *J. Mater. Chem.*, 1998, **8**, 1743-1748.
27. J. Shan and H. Tenhu, *Chemical Communications*, 2007, 4580-4598.
28. M. El-Rafie, M. El-Naggar, M. Ramadan, M. M. Fouda, S. S. Al-Deyab and A. Hebeish, *Carbohydrate Polymers*, 2011, **86**, 630-635.
29. S. S. Shankar, A. Rai, A. Ahmad and M. Sastry, *Journal of colloid and interface science*, 2004, **275**, 496-502.
30. S. Manna, S. K. Batabyal and A. K. Nandi, *The Journal of Physical Chemistry B*, 2006, **110**, 12318-12326.
31. J. AlanáCreighton, *Journal of the Chemical Society, Faraday Transactions*, 1991, **87**, 3881-3891.
32. A. Henglein and D. Meisel, *Langmuir*, 1998, **14**, 7392-7396.
33. R. R. Naik, S. J. Stringer, G. Agarwal, S. E. Jones and M. O. Stone, *Nature materials*, 2002, **1**, 169-172.
34. P. Mulvaney, *Langmuir*, 1996, **12**, 788-800.
35. J. A. Lopez-Sanchez, N. Dimitratos, C. Hammond, G. L. Brett, L. Kesavan, S. White, P. Miedziak, R. Tiruvalam, R. L. Jenkins and A. F. Carley, *Nature Chemistry*, 2011, **3**, 551-556.
36. X. Zhang and Z. Su, *Advanced Materials*, 2012, **24**, 4574-4577.

37. D. M. Dotzauer, J. Dai, L. Sun and M. L. Bruening, *Nano letters*, 2006, **6**, 2268-2272.
38. V. Vidhu and D. Philip, *Micron*, 2014, **56**, 54-62.
39. C. Corredor, M. D. Borysiak, J. Wolfer, P. Westerhoff and J. D. Posner, *Environmental Science & Technology*, 2015, **49**, 3611-3618.
40. T. Shahwan, S. Abu Sirriah, M. Nairat, E. Boyacı, A. Eroğlu, T. Scott and K. Hallam, *Chemical Engineering Journal*, 2011, **172**, 258-266.
41. M. A. Rauf, M. A. Meetani, A. Khaleel and A. Ahmed, *Chemical Engineering Journal*, 2010, **157**, 373-378.